Dalton Transactions

Photophysical properties of three-coordinate heteroleptic Cu(I) β-diketiminate triarylphosphine complexes

Journal:	*Dalton Transactions*
Manuscript ID	DT-ART-09-2024-002681.R1
Article Type:	Paper
Date Submitted by the Author:	30-Oct-2024
Complete List of Authors:	Kumar, Ashish; University of Houston, Department of Chemistry Kim, Dooyoung; University of Houston, Department of Chemistry Nguyen, Giao; University of Houston, Department of Chemistry Jiang, Chenggang; University of Houston, Department of Chemistry Chakraborty, Soumi; University of Houston, Department of Chemistry Teets, Thomas; University of Houston, Department of Chemistry

PAPER

Photophysical properties of three-coordinate heteroleptic Cu(I) β-diketiminate triarylphosphine complexes†

Received 00th January 20xx,
Accepted 00th January 20xx

DOI: 10.1039/x0xx00000x

Ashish Kumar, Dooyoung Kim, Giao Nguyen, Chenggang Jiang, Soumi Chakraborty, and Thomas S. Teets*

A series of heteroleptic copper(I) β-diketiminate triarylphosphine complexes is reported, having the general formula Cu(R^1NacNac^{R2})(PPh^X_3), where R^1NacNac^{R2} is a substituted β-diketiminate and PPh^X_3 is a triphenylphosphine derivative. A total of five different R^1NacNac^{R2} ligands and three different triarylphosphines are used to assemble the nine complexes. The syntheses, X-ray crystal structures, cyclic voltammograms, and UV–vis absorption spectra of all compounds are described. Whereas most of the compounds are weakly luminescent or only luminesce at 77 K, the four complexes with the more sterically encumbered β-diketiminate ligands, with methyl or isopropyl substituents at the 2- and 6-positions of the *N*-phenyl rings, exhibit weak room-temperature photoluminescence with peaks between 519 and 566 nm and long excited-state lifetimes in the range of 15–70 μs. The sterically encumbering substituents in this subset have subtle effects on the UV–vis absorption maximum, which red shifts slightly as the steric bulk increases, as well as significant effects on the photoluminescence lifetime, which is observed to increase as the steric bulk is augmented. Substituents on the triarylphosphine also influence the excited-state dynamics in the bulky complexes, with the more electron-rich tris(4-methoxyphenyl)phosphine (PPh^{OMe}_3) giving longer-excited-state lifetimes compared to triphenylphosphine (PPh_3) when the same R^1NacNac^{R2} ligand is used.

Introduction

Photosensitizers capture solar energy and convert it to a chemical potential,[1,2] with many applications possible, photovoltaics and photocatalysis being most prevalent.[3–6] Molecular photosensitizers based on the 4*d* and 5*d* transition metals ruthenium[7–10] and iridium[11–14] have been used widely, but these metals are scarce and costly. Sustainable alternatives such as metal-free organic molecules[15–18] and first-row transition-metal complexes[19–22] have been increasingly explored. Despite their economic advantages, the performance of 3*d* metal photosensitizers is often limited by one or more factors, such as weak absorption in the visible spectrum, poor stability, and short-lived excited states.

Copper(I) has gained much recent attention in the design of charge-transfer photosensitizers, in large part due to its d^{10} valence electronic configuration, avoiding the low-lying metal-centered states that plague other 3*d* photosensitizers and giving access to low-energy metal-to-ligand charge transfer (MLCT) states. There are, nevertheless, several excited-state deactivation pathways that must be considered when designing copper(I) photosensitizers, which mainly involve structural distortion in the excited state.[23–25] One interesting feature of copper(I) is that its coordinative flexibility has allowed researchers to design photosensitizers with a variety of coordination geometries, which impacts the ground-state electronic structure and the excited-state dynamics. Classically, four-coordinate, bis-chelate distorted tetrahedral complexes have received the most attention in the development of Cu(I) photosensitizers, well-known to undergo a pseudo Jahn-Teller flattening distortion in the MLCT excited state.[26–29] In the opposite extreme, luminescent linear two-coordinate Cu(I) complexes have been recently popularized,[30,31] applied in one study as solar photsensitizers.[32]

Most relevant to the present work, there are a few classes of three-coordinate Cu(I) photosensitizers in the literature. One of the initial reports of a luminescent three-coordinate mononuclear copper(I) complex appeared in 2003.[33] Three-coordinate halide-terminated diphosphine complexes can be strongly luminescent in solution or the solid state,[34,35] leading to applications in OLEDs.[34] Given the coordinative flexibility of copper(I), from a synthetic standpoint increased steric bulk on the ligands can favor the three-coordinate geometry over four-coordinate[36,37] or dinuclear alternatives.[38] Generally, the molecular geometry in three-coordinate Cu(I) complexes is distorted trigonal planar, often described as Y-shaped, but a T-shaped geometry is possible with trans-spanning chelating ligands.[39,40] Much like their four-coordinate predecessors, the excited-state distortion pathways of three-coordinate Cu(I) complexes have been well characterized.[35,41]

Department of Chemistry, University of Houston, 3585 Cullen Blvd, Room 112, Houston, TX, 77204-5003, USA. E-mail: tteets@uh.edu

†Electronic Supplementary Information (ESI) available: X-ray crystallography summary tables, NMR spectra, additional photophysical data and cyclic voltammograms, results from DFT calculations. CCDC 2382410–2382413 and 2382415–2382419. See DOI: 10.1039/x0xx00000x

Our group has developed Cu(I) substituted β-diketiminate (NacNac) complexes as charge-transfer photosensitizers; most previous studies on Cu-NacNac complexes were conducted in the context of small-molecule activation.[42] Our initial efforts focused on four-coordinate heteroleptic complexes pairing NacNac and diimine ligands, which exhibited tunable HOMO–LUMO gaps[43,44] and excited-state dynamics that were responsive to the steric profile of both the NacNac and diimine ligands.[45] More recently, we have described three-coordinate Cu-NacNac complexes terminated with monodentate isocyanide acceptor ligands, in which the excited-state lifetimes and photoredox reactivity could be enhanced by triplet-triplet energy transfer with pyrene-substituted isocyanides[46] or by steric effects in *m*-terphenylisocyanides.[47] In this work, we explore the possibility of using triarylphosphines as the neutral donor ligands in three-coordinate copper(I) β-diketiminate charge-transfer chromophores. Phosphines have an empty σ* orbital that give them π-accepting capabilities,[48,49] and we hypothesized that this orbital could serve as the acceptor orbital in a charge-transfer excited state. There are previously reported examples of Cu(I) β-diketiminate triphenylphosphine complexes, but there is no description of their photophysical properties.[50,51] Here we describe a series of nine complexes with the general formula Cu(R^1NacNac^{R2})(PPh^X_3). R^1NacNac^{R2} is the β-diketiminate with variable substituents at the *N*-positions (R^1) and the backbone positions (R^2), and PPh^X_3 is triphenylphosphine or a substituted variant with electron-donating (X = OMe) or electron-withdrawing (X = F) groups at the 4-positions of the phenyl rings. The molecular structures of all nine complexes were characterized by single-crystal X-ray diffraction, and this work also includes their electrochemical properties, measured via cyclic voltammetry, and detailed photophysical analysis. Most of the compounds are weakly photoluminescent, some at room temperature and some only at 77 K. We find that steric effects on the R^1NacNac^{R2} are particularly important in dictating the photophysical properties, as the four members of the series with bulky β-diketiminate ligands are the only ones to exhibit room-temperature photoluminescence. The complexes that do luminesce at room temperature have long excited-state lifetimes on the order of 10^{-5} s, clearly indicating that phosphorescence is occurring.

Results and discussion

Synthesis of Cu(R^1NacNac^{R2})(PPh^X_3) complexes

The synthesis of heteroleptic Cu(R^1NacNac^{R2})(PPh^X_3) complexes is summarized in Scheme 1. To prepare complexes **Cu1–Cu9**, CuO^tBu was first treated with the protonated β-diketiminate proligand, and after stirring at room temperature for 1–2 hours the phosphine ligand was added; a substoichiometric amount of PPh^X_3 (0.4–0.6 equivalents) was used, to avoid formation of four-coordinate, bis-phosphine byproducts. After addition of the phosphine, reactions were allowed to proceed for 24–72 h at room temperature or 60–70 °C. The nine compounds described here use five different R^1NacNac^{R2} ligands. Four of those have backbone methyl groups (R^2 = Me), with the *N*-substituents either phenyl (PhNacNac^{Me}), cyclohexyl

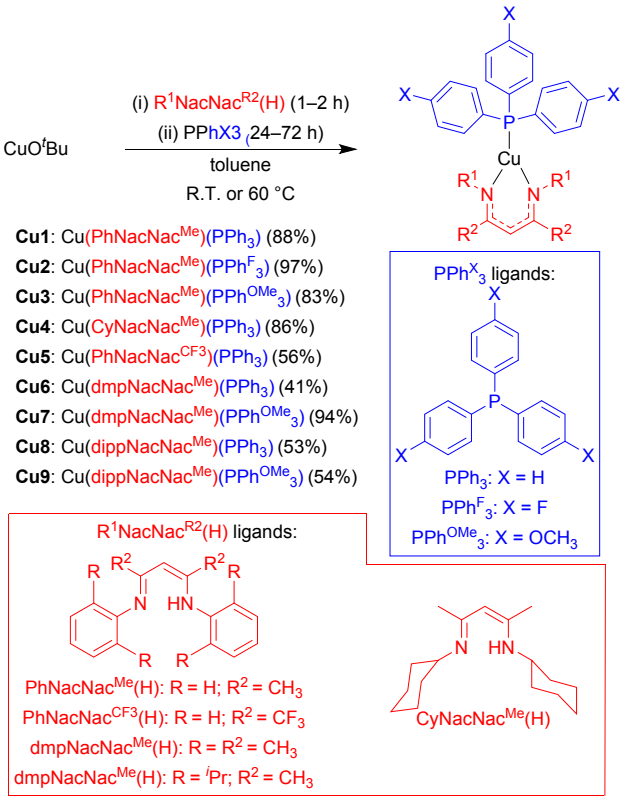

Scheme 1 General scheme for the synthesis of complexes **Cu1**–**Cu9**.

(CyNacNac^{Me}), 2,6-dimethylphenyl (dmpNacNac^{Me}), or 2,6-diisopropylphenyl (dippNacNac^{Me}). One β-diketiminate with a fluorinated backbone, PhNacNac^{CF3}, was used in one of the compounds (**Cu5**). The three phosphines used are PPh_3 and two closely related variants substituted with electron-donating (OCH_3, PPh^{OMe}_3) or electron-withdrawing (F, PPh^F_3) groups at the 4-positions of the phenyl rings. The target products were isolated in 41–97% yield and handled in an inert-atmosphere glovebox due to moisture and air sensitivity. The structures and bulk purity of the synthesized complexes were validated by ^{1}H, ^{19}F (complexes with PhNacNac^{CF3} or PPh^F_3) and ^{31}P{^{1}H} NMR spectroscopy (Fig. S1–S20).

The molecular structures of all complexes were further characterized by X-ray crystallography. We note that crystal structures of **Cu6** and **Cu8** have been previously reported[50,51] and are included here for completeness. Structures are shown in Fig. 1 with hydrogen atoms and solvent molecules omitted for clarity, and crystallographic parameters are summarized in the Supporting Information, Tables S1–S5. The planar three-coordinate geometries are best described as Y-shaped, and similar bond metrics are observed across the series, with no systematic dependence on the electronic nature of the phosphine or the steric profile of the R^1NacNac^{R2} ligand. In any given compound, the two Cu–N distances differ by no more than 0.02 Å, indicating symmetric bidentate coordination of the R^1NacNac^{R2} ligand. The Cu–P internuclear distances are likewise nearly identical in all complexes, spanning 2.1658(6)–2.2012(6) Å, and even with the more sterically encumbered β-

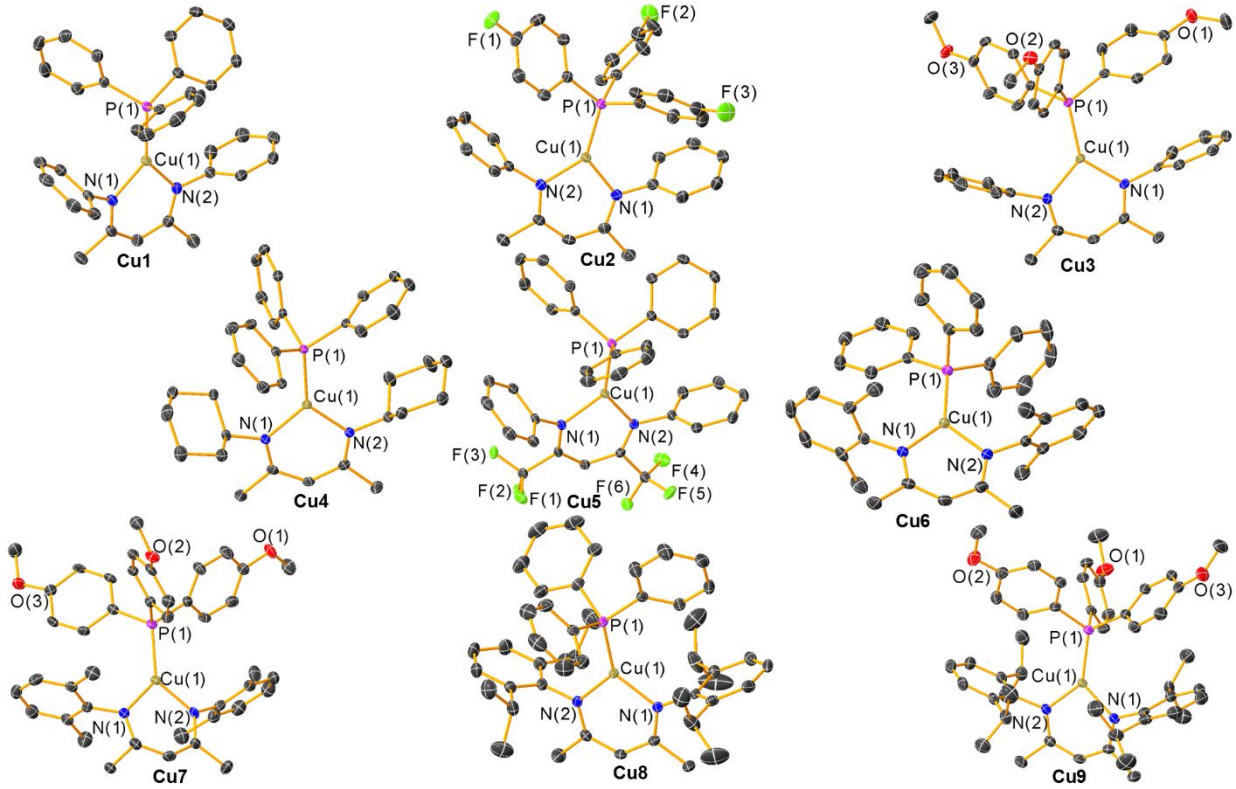

Fig. 1. Molecular structures of the complexes **Cu1**–**Cu9** determined by single crystal X-ray diffraction. Thermal ellipsoids are drawn at the 50% probability level, except for **Cu6**, for which data was collected at higher temperature (183 K instead of 123 K) and ellipsoids are thus shown at 30% probability. Hydrogen atoms and solvent molecules have been omitted for clarity.

diketiminates (**Cu7–Cu9**) there is no noticeable elongation, consistent with tight binding of the phosphine.

Electrochemistry

The electrochemical behavior of **Cu1**–**Cu9** was evaluated by cyclic voltammetry. The voltammograms of **Cu1–Cu5** are shown in Fig. S26–S30 and summarized in Table S7. Those of **Cu6**–**Cu9**, which are photoluminescent at room temperature (see below), are collected in Fig. 2 with the redox potentials summarized in Table 1. In most cases, the redox events are electrochemically irreversible. The oxidation waves of these Cu(I) complexes can be formalized as Cu^{II}/Cu^{I} couples, although on the basis of electronic structure calculations on related Cu(I) β-diketiminate complexes[43,46] and those we report here (see below), we note there is significant HOMO electron density on the R^1NacNac^{R2} ligand, meaning there is also significant redox activity of this ligand. In **Cu6–Cu9** (Table 1) the peak potentials are slightly more positive than ferrocenium/ferrocene couple, and substituents on the β-diketiminate ligand can drive this potential substantially more negative (CyNacNac^{Me} complex **Cu4**) or positive (PhNacNac^{CF3} complex **Cu5**). In most cases, scanning to negative potentials fails to reveal a reductive wave within the solvent window. In complexes **Cu6** (E^{red} = −3.42 V) and **Cu8** (E^{red} = −3.34 V) a reversible wave was observed, with the potentials signifying very shallow (high-energy) LUMOs in these compounds.

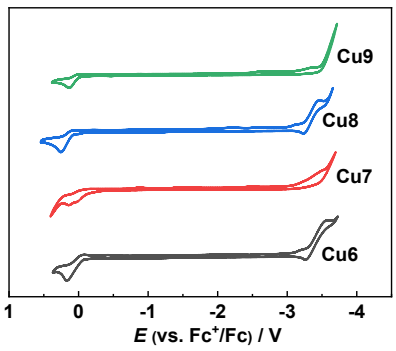

Fig. 2. Overlaid cyclic voltammogramms of **Cu6**–**Cu9**. The CVs were recorded in THF with 0.1 M NBu_4PF_6 as the supporting electrolyte. Potentials were referenced against an internal standard of ferrocene.

Table 1 Summary of the electrochemical data of **Cu6-Cu9**[a]

Complex	E^{ox} / V ($[Cu]^+/[Cu]$)	E^{red} / V ($[Cu]/[Cu]^-$)	ΔE_{H-L} / eV[b]
Cu6	0.17	−3.42	3.59
Cu7	0.14	–	–
Cu8	0.26	−3.34	3.60
Cu9	0.13	–	–

[a] In all cases for E^{ox}, peak anodic potentials, $E_{p,a}$, are reported. For E^{red}, half-wave potentials ($E_{1/2}$) are reported. [b] Estimated electrochemical HOMO–LUMO gap, determined as $E^{ox} - E^{red}$.

Photophysical properties

UV–vis absorption spectra of **Cu1–Cu5** are shown in Fig. S21–S25 and summarized in Table S6, whereas those of luminescent

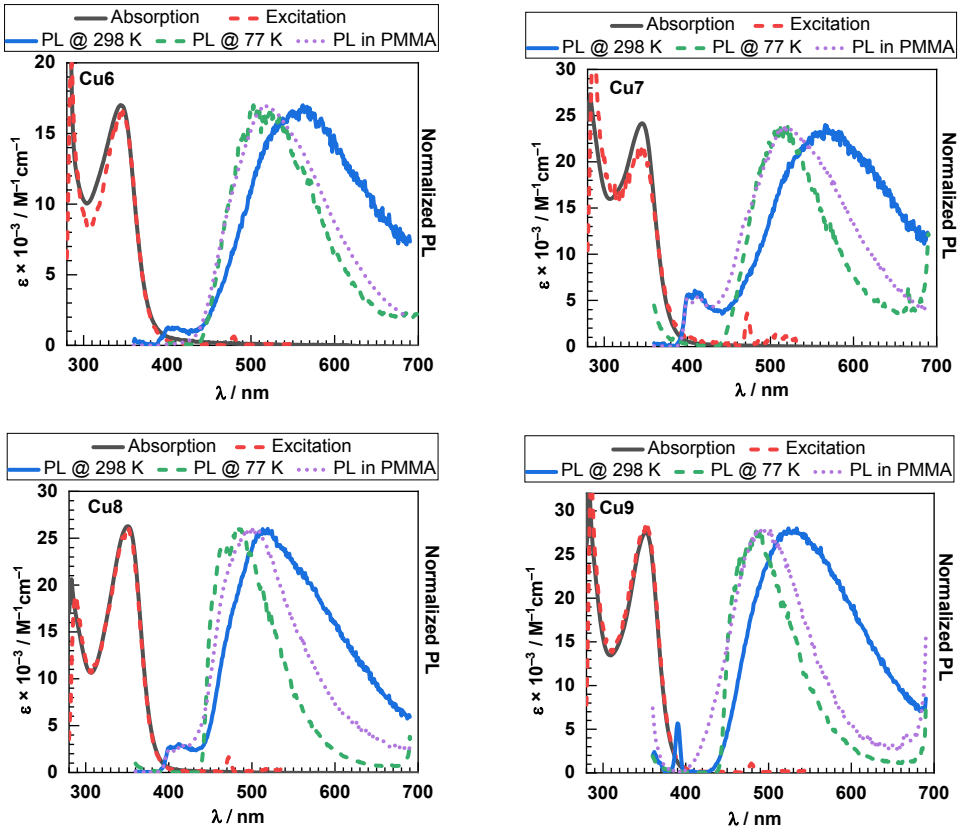

Fig. 3. Overlaid UV-vis absorption, excitation, and photoluminescence spectra of **Cu6–Cu9**. UV–vis absorption (black solid line) and excitation (red dashed line) were recorded in toluene at 298 K. Photoluminescence spectra were recorded at 298 K in toluene (blue solid line), 77 K in toluene (green dashed line), and 298 K at 2 wt% in PMMA film (purple dotted line).

Table 2 Summary of the photophysical data of the emissive complexes **Cu6**-**Cu9**

	UV–vis absorption	PL in toluene (298 K)			PL in toluene (77 K)	PL in PMMA (298 K)
Complex	λ_{max} / nm ($\varepsilon \times 10^{-3}$ / $M^{-1}cm^{-1}$)	λ_{max} / nm	τ / μs	Φ_{PL}	λ_{max} / nm	λ_{max} / nm
Cu6	344 (17)	562	15	0.4%	503	517
Cu7	345 (24)	566	43	0.4%	521	518
Cu8	351 (26)	519	62	0.1%	484	501
Cu9	352 (28)	524	70	0.1%	485	491

complexes **Cu6–Cu9** are in Fig. 3 and summarized in Table 2. The absorption spectra all show a single dominant peak in near-UV, between 317 and 385 nm with ε = 7.8–27 × 10^3 $M^{-1}cm^{-1}$. This feature is strongly responsive to the substitution on the $R^1NacNac^{R2}$ ligand, and little influenced by the phosphine substituents. Specifically, this band appears at 353–355 nm in the $PhNacNac^{Me}$ complexes (**Cu1–Cu3**), shifting minimally in the alkyl-substituted analogues with $dmpNacNac^{Me}$ (**Cu6** and **Cu7**, 344 and 345 nm, respectively) or $dippNacNac^{Me}$ (**Cu8** and **Cu9**, 352 nm in both cases). Much more pronounced shifts are observed in the $CyNacNac^{Me}$ complexes (**Cu4**), where the maximum absorption blue shifts to 317 nm, and in **Cu5** ($PhNacNac^{CF3}$), where the maximum red shifts to 385 nm. DFT calculations (see below) indicate that these transitions are charge-transfer in nature, involving filled (donor) orbitals on the Cu-NacNac core and unoccupied (acceptor) orbitals on the triarylphosphine. The strong dependence of the electronic transition on the $R^1NacNac^{R2}$ substituents indicates that the donor orbital energies are strongly influenced by the $R^1NacNac^{R2}$ substitution pattern, consistent with the redox potentials measured by cyclic voltammetry. The negligible influence of the phosphine substituents suggests the acceptor orbital energies in this set of triarylphosphine ligands are all very similar.

The Cu complexes are weakly photoluminescent; in **Cu1–Cu4** there is weak, broad PL in toluene glass at 77 K and in **Cu5** no luminescence is observed at room temperature or 77 K. The complexes with the sterically encumbered β-diketiminate ligands, **Cu6**–**Cu9**, do exhibit photoluminescence at 298 K, as shown in Fig. 3 and summarized in Table 2. The peak PL wavelengths depend slightly on the identity of the β-diketiminate, occurring near 560 nm in $dmpNacNac^{Me}$ complexes **Cu6** and **Cu7**, blue-shifting to near 520 nm in $dippNacNac^{Me}$ complexes **Cu8** and **Cu9.** The shoulder around 400 nm in the spectra of **Cu6–Cu8** is due to an instrumental artifact, with the intensity of this feature decreasing as the

concentration of the copper complex increases. Low photoluminescence quantum yields of 0.4% (**Cu6** and **Cu7**) and 0.1% (**Cu8** and **Cu9**) are observed for these four complexes. Excitation spectra, also given in Fig. 3, overlay well with the UV–vis absorption spectra and indicate the PL originates from the respective copper complex and that Kasha's rule is followed.

Photoluminescence lifetimes, also recorded at room temperature in toluene, are all on the order of 10^{-5} s. These long lifetimes indicate that the photoluminescence can be assigned as phosphorescence, originating from a triplet excited state. The PL decay lifetime is responsive to the steric profile of the β-diketiminate and the substituents on the phosphine. The bulkiest isopropyl-substituted dippNacNac^{Me} complexes, **Cu8** and **Cu9**, have the longest PL lifetimes in the series at 62 μs and 70 μs, respectively. In contrast, the methyl-substituted dmpNacNac^{Me} analogues have τ = 15 μs (**Cu6**) and 43 μs (**Cu7**). The lengthening of the lifetimes with increasing steric bulk is consistent with restriction of the excited-state distortion by the sterically encumbering groups, as has been observed in many other classes of copper(I) charge-transfer chromophores.[45,47,53–55] In addition, in both pairs of complexes with the same β-diketiminate ligand (**Cu6**/**Cu7** and **Cu8**/**Cu9**), the methoxy-substituted PPh$^{OMe}_3$ analogue has the longer lifetime; the origin of this effect is unclear, since the remote *para* location of the methoxy substituents should not have a significant influence on the steric profile (see crystal structures in Fig. 1), and the electrochemical and photophysical data suggest that the methoxy groups are also electronically benign.

Photoluminescence in complexes **Cu6**–**Cu9** was also recorded at 2 wt% in poly(methyl methacrylate) films at room temperature, and in toluene glass at 77 K. In both of these rigid media the PL spectrum maintains a broad, featureless profile and a significant rigidochromic blue shift is also observed as well. Both of these observations are consistent with the photoluminescence originating from a charge-transfer excited state, abbreviated generally as ^{3}CT.

DFT Calculations

Density functional theory (DFT) calculations were performed on complex **Cu6** to determine the nature of the frontier orbitals and electronic transitions. Given the similarity of the cyclic voltammograms, UV–vis absorption spectra, and PL features of **Cu6**–**Cu9**, we presume that the insights gleaned from DFT apply to all of the luminescent compounds in this series. Fig. 4 presents contour plots of the HOMO and LUMO along with other orbitals involved in the most intense electronic transitions. A more complete set of frontier orbital contour plots is shown in Fig. S31. The HOMO (−4.87 eV) is mainly a π orbital localized on the core of the dmpNacNac^{Me} ligand with minor contribution of the copper center, whereas the LUMO (−1.11 eV) is mostly localized on the phenyl rings of the PPh$_3$ ligand. The corresponding HOMO–LUMO energy gap of 3.76 eV is in good agreement with the experimentally determined electrochemical HOMO–LUMO gap (3.59 eV, Table 1).

Time-dependent density functional theory (TDDFT) was used to evaluate the major electronic transitions in **Cu6**. The simulated spectrum is shown in Fig. S32 and consists of several

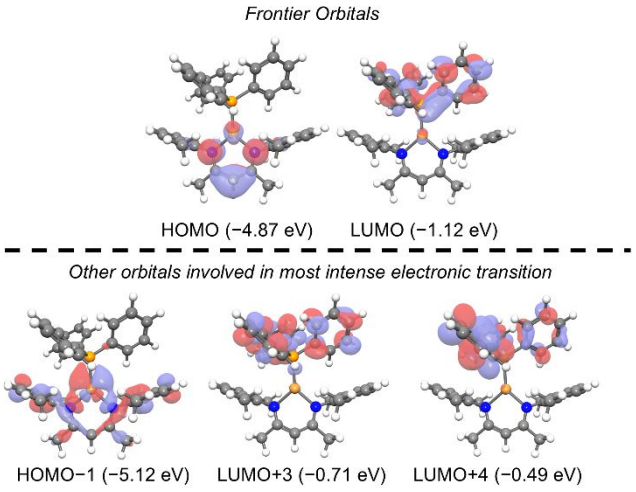

Fig. 4. Frontier molecular orbitals (isovalue 0.08) of **Cu6** (computed at uB3LYP/6-31+g(d) level in toluene) and those associated with the most intense transition in the computed UV–vis absorption spectrum.

overlapping transitions, the most prominent of which are summarized in Table S8. The most intense transition involves HOMO−1 to LUMO+3 and HOMO to LUMO+4 excitations. The other frontier orbitals involved in this transition are also shown in Fig. 4. In this excited state, the donor orbitals (HOMO and HOMO−1) are primarily localized on the dmpNacNac^{Me} with the acceptor orbitals (LUMO+3 and LUMO+4) on the phosphine, corroborating that the low-energy transitions are aptly described as charge-transfer in nature.

Conclusions

A series of heteroleptic three coordinate Cu(I) β-diketiminate triarylphosphine complexes was synthesized, to evaluate the effects that phosphine capping ligands have on the photophysical properties of this emerging class of charge-transfer chromophores. Electronic absorption bands occur in the near-UV region, tailing out to 400 nm in some cases. Four of the complexes, those with the most sterically encumbered β-diketiminate ligands, exhibit weak photoluminescence in solution at room temperature, occurring between ca. 520–560 nm for these complexes. We conclude that the increased steric bulk in this subset of compounds prevents excited-state distortion, allowing phosphorescence to occur with long lifetimes between 15 μs (**Cu6**) and 70 μs (**Cu9**). Substitution on the phosphine ligand also influences the PL lifetime; replacing PPh$_3$ with PPh$^{OMe}_3$ increases the lifetime significantly in both pairs of luminescent complexes. In conclusion, this work shows that while triarylphosphine ligands shift the absorption bands to shorter wavelengths, which is detrimental to the potential of these complexes as charge-transfer photosensitizers, they can promote long excited-state lifetimes.

Experimental section

Materials

All reactants and solvents for synthetic procedures were measured and purification steps were executed in a nitrogen-filled glovebox operating at < 1 ppm of O_2 and < 1 ppm of H_2O. Solvents for reactions, electrochemical measurements, and photophysical measurements were dried by the method of Grubbs,[56] passing through dual alumina columns on a commercial solvent purification system and stored over 3 Å molecular sieves before use. NMR solvents were also stored in 3 Å molecular sieves. Tetrabutylammonium hexafluorophosphate (NBu_4PF_6) and ferrocene were purified by recrystallization from hot ethanol and sublimation, respectively, before use in electrochemical measurements. All starting materials and reagents were purchased from commercial sources and used without any further purification, unless otherwise stated. Copper(I) *tert*-butoxide (CuO^tBu)[57] and the β-diketiminate ligands $PhNacNac^{Me}(H)$,[58] $CyNacNac^{Me}(H)$,[59] $PhNacNac^{CF3}(H)$,[58] $dmpNacNac^{Me}(H)$,[60] and $dippNacNac^{Me}(H)$,[60] were synthesized according to previously reported procedures.

Physical methods

NMR spectra (presented in Fig. S1–S20 in the ESI†) were obtained at room temperature using a JEOL ECA-400 or ECA-600 NMR spectrometer. UV–vis absorption spectra were recorded in toluene solutions in screw-capped quartz cuvettes using an Agilent Cary 8454 UV–vis spectrometer. Cyclic voltammetry (CV) measurements were carried out with a CH instruments 602E potentiostat interfaced with a nitrogen-filled glovebox via wire feedthroughs. A 3 mm diameter glassy carbon working electrode and a platinum wire counter electrode were used. The pseudoreference electrode consisted of a silver wire immersed in a solution containing 0.1 M NBu_4PF_6 in THF. Samples were dissolved in THF with 0.1 M NBu_4PF_6 as a supporting electrolyte. Potentials were referenced against ferrocene as an internal standard. Photoluminescence and excitation spectra were obtained using a Horiba FluoroMax-4 spectrofluorometer. Room-temperature PL samples were housed in 1 cm quartz cuvettes with septum-sealed screw caps. For PL measurements at 77 K, the sample was contained in a custom quartz EPR tube with a high-vacuum valve. To cool the sample, it was immersed in liquid nitrogen contained in a quartz dewar sample holder specifically designed for the fluorimeter's sample chamber. Samples for these measurements were prepared inside a nitrogen-filled glovebox using dry and deoxygenated solvents to exclude air. Luminescence lifetimes were measured with a Horiba DeltaFlex Lifetime System, using 330 nm pulsed diode excitation. Emission wavelengths were selected by using appropriate long-pass filters, and the decay trace was fitted using the instrument's analysis software or the software Origin 2020b. Photoluminescence quantum yields for all complexes were measured relative to quinine sulfate, which has a reported fluorescence quantum yield (Φ_F) of 0.52.[61] The quantum yields of the copper-based complexes (Φ_x) were calculated using Equation 1 below, where Φ_{st} = the quantum yield of the standard, m_x = the slope of integrated emission intensity versus absorbance for the samples, m_{st} = the slope of emission intensity versus absorbance for the standard compound, and η_x and η_{st} are the refractive indexes of the solvents of the sample and standard, respectively.

$$\Phi_x = \Phi_{st}\left[\frac{m_x}{m_{st}}\right]\left[\frac{\eta_x}{\eta_{st}}\right]^2 \quad (1)$$

X-ray crystallography details

Single crystals were grown by vapor diffusion of pentane into a concentrated THF solution or evaporation of a diethyl ether solution. Crystals were mounted on a Bruker Apex II three-circle diffractometer using Mo Kα radiation (λ = 0.71073 Å). The data were collected at 123 K for all structures except **Cu6**, which was measured at 183 K. After collection the data was processed and refined within the APEXII software. Structures were solved by intrinsic phasing in SHELXT and refined by standard difference Fourier techniques in the program SHELXL.[62] Hydrogen atoms were placed in calculated positions using the standard riding model and refined isotropically; all nonhydrogen atoms were refined anisotropically. Crystallographic details are summarized in Tables S1–S5.

Computational details

DFT calculations on **Cu6** were performed at the B3LYP[63] level of theory using Gaussian16 quantum chemistry package.[64] We used LANL2DZ[65] basis set with the relativistic effective core potential for Cu and 6-31+g(d) basis for other elements (H, C, N, P). The geometries were optimized without any symmetry constraints. The crystal structure was used as the initial input for the geometry optimization. The molecular orbitals were visualized using IQmol. Time-dependent density functional theory (TDDFT) was employed to calculate electronic excitation energies as implemented in Gaussian 16. We used the B3LYP functional in combination with 6-31+g(d) basis set. The conductor-like polarizable continuum model, CPCM was used to model toluene solvation.[66]

General procedure for synthesis of $Cu(R^1NacNac^{R2})(PPh^X_3)$

In a nitrogen-filled glovebox, a mixture of CuO^tBu and 1 equivalent of the respective protonated $R^1NacNac^{R2}(H)$ was stirred in 3 mL of toluene, for a period of 1–2 h. In a separate vial, 0.4–0.6 equiv. of the respective triarylphosphine ligand was dissolved in 3 mL of toluene. The toluene solution of the phosphine was added to the mixture of CuO^tBu and $R^1NacNac^{R2}(H)$ solution via a pipette. The mixture was stirred for 24–72 h at room temperature or 60–70 °C. The resulting solution was passed through a pad of glass fiber, and all volatiles were removed under vacuum. The crude product was washed with hexane or pentane and dried under a vacuum before characterization.

Cu1 ($Cu(PhNacNac^{Me})(PPh_3)$). Prepared by the general procedure using CuO^tBu (55 mg, 0.40 mmol), $PhNacNac^{Me}(H)$ (100 mg, 0.399 mmol), and PPh_3 (63 mg, 0.24 mmol). The mixture was stirred at room temperature for 24 h. Yield: 122 mg (88%). ^1H NMR (600 MHz, C_6D_6): δ (ppm) 6.95–7.00 (m, 9H, Ar*H*), 6.86–6.93 (m, 14H, Ar*H*), 6.76–6.81 (m, 2H, Ar*H*), 5.09 (s, 1H, N–C(CH_3)=C*H*–C(CH_3)=N), 2.00 (s, 6H, CH_3). $^{31}P\{^1H\}$ NMR (243 MHz, C_6D_6): δ (ppm) 4.4 (s).

Cu2 (Cu(PhNacNac^{Me})(PPh$^{F}_3$)). Prepared by the general procedure using CuO^{t}Bu (55 mg, 0.40 mmol), PhNacNac^{Me}(H) (100 mg, 0.399 mmol), and PPh$^{F}_3$ (79 mg, 0.24 mmol). The mixture was stirred at room temperature for 24 h. Yield: 147 mg (97%). ^{1}H NMR (400 MHz, C_6D_6): δ (ppm) 6.80–6.88 (m, 8H, Ar*H*), 6.66–6.75 (m, 8H, Ar*H*), 6.57–6.62 (m, 6H, Ar*H*), 5.07 (s, 1H, N–C(CH$_3$)=C*H*–C(CH$_3$)=N), 1.97 (s, 6H, C*H*$_3$). ^{19}F NMR (470 MHz, C_6D_6): δ (ppm) −110.47 (m). ^{31}P{^{1}H} NMR (202 MHz, C_6D_6): δ (ppm) 1.3 (s).

Cu3 (Cu(PhNacNac^{Me})(PPh$^{OMe}_3$)). Prepared by the general procedure using CuO^{t}Bu (55 mg, 0.40 mmol), PhNacNac^{Me}(H) (100 mg, 0.399 mmol), and PPh$_3^{OMe3}$ (85 mg, 0.24 mmol). The mixture was stirred at room temperature for 24 h. Yield: 134 mg (83%). ^{1}H NMR (400 MHz, C_6D_6): δ (ppm) 6.91−7.05 (m, 14H, Ar*H*), 6.77−6.82 (m, 2H, Ar*H*), 6.55–6.62 (m, 6H, Ar*H*), 5.12 (s, 1H, N–C(CH$_3$)=C*H*–C(CH$_3$)=N), 3.24 (s, 9H, OC*H*$_3$), 2.03 (s, 6H, C*H*$_3$). ^{31}P{^{1}H} NMR (162 MHz, C_6D_6): δ (ppm) 0.8 (s).

Cu4 (Cu(CyNacNac^{Me})(PPh$_3$)). Prepared by the general procedure using CuO^{t}Bu (55 mg, 0.40 mmol), CyNacNac(H) (105 mg, 0.400 mmol), and PPh$_3$ (63 mg, 0.24 mmol). The mixture was stirred at room temperature for 24 h. Yield: 121 mg (86 %). ^{1}H NMR (600 MHz, C_6D_6): δ (ppm) 7.62–7.69 (m, 6H, Ar*H*), 6.99–7.03 (m, 9H, Ar*H*), 4.73 (s, 1H, N–C(CH$_3$)=C*H*–C(CH$_3$)=N), 3.46 (tt, *J* = 11, 3.9 Hz, 2H, C*H*), 2.18 (s, 6H, C*H*$_3$), 1.80–1.86 (m, 4H, C*H*$_2$), 1.41–1.44 (m, 4H, C*H*$_2$), 1.31–1.38 (m, 4H, C*H*$_2$), 1.25 (dt, *J* = 12.9, 3.3 Hz, 2H, C*H*$_2$), 1.15 (qt, *J* = 13, 3.7 Hz, 4H, C*H*$_2$) 0.14 (qt, *J* = 13, 3.9 Hz, 2H, *CH*$_2$). ^{31}P{^{1}H} NMR (243 MHz, C_6D_6): δ (ppm) 3.5 (s).

Cu5 (Cu(PhNacNac^{CF3})(PPh$_3$)). Prepared by the general procedure using CuOtBu (55 mg, 0.40 mmol), PhNacNac^{CF3}(H) (143 mg, 0.399 mmol), and PPh$_3$ (53 mg, 0.20 mmol). The mixture was stirred at 70 °C for 24 h. Yield: 77 mg (56%). ^{1}H NMR (600 MHz, C_6D_6): 6.94 (t, *J* = 7.5 Hz, 3H, Ar*H*), 6.89 (d, *J* = 7.8 Hz, 4H, Ar*H*), 6.85–6.74 (m, 16H, Ar*H*), 6.71 (t, *J* = 7.4 Hz, 2H, Ar*H*), 6.35 (s, 1H, N–C(CF$_3$)=C*H*–C(CF$_3$)=N). ^{19}F NMR (565 MHz, C_6D_6): δ (ppm) −58.83 (s). ^{31}P{^{1}H} NMR (243 MHz, C_6D_6): δ (ppm) 4.6 (s).

Cu6 (Cu(dmpNacNac^{Me})(PPh$_3$)). Prepared by the general procedure using CuO^{t}Bu (41 mg, 0.30 mmol), dmpNacNac(H) (92 mg, 0.30 mmol), and PPh$^{OMe}_3$ (47 mg, 0.18 mmol). The mixture was stirred at 60 °C for 24 h. Yield: 41 mg (41%). ^{1}H NMR (600 MHz, C_6D_6): δ (ppm) 6.99–6.85 (m, 21H, Ar*H*), 5.08 (s, 1H, N–C(CH$_3$)=C*H*–C(CH$_3$)=N), 2.15 (s, 12H, Ar−C*H*$_3$), 1.76 (s, 6H, N–C(C*H*$_3$)=CH–C(C*H*$_3$)=N). ^{31}P{^{1}H} NMR (162 MHz, C_6D_6): δ (ppm) 5.5 (s).

Cu7 (Cu(dmpNacNac^{Me})(PPh$^{OMe}_3$)). Prepared by the general procedure using CuO^{t}Bu (41 mg, 0.30 mmol), dmpNacNac^{Me}(H) (92 mg, 0.30 mmol), and PPh$^{OMe}_3$ (42 mg, 0.12 mmol). The mixture was stirred at RT for 48 h. Yield: 94 mg (94%). ^{1}H NMR (400 MHz, C_6D_6): δ (ppm) 6.86–6.98 (m, 12H, Ar*H*), 6.63–6.58 (m, 6H, Ar*H*), 5.10 (s, 1H, N–C(CH$_3$)=C*H*–C(CH$_3$)=N), 3.24 (s, 9H, OC*H*$_3$), 2.23 (s, 12H, Ar-*CH*$_3$), 1.78 (s, 6H, N–C(C*H*$_3$)=CH–C(C*H*$_3$)=N). ^{31}P{^{1}H} NMR (202 MHz, C_6D_6): δ (ppm) 1.8 (s).

Cu8 (Cu(dippNacNac^{Me})(PPh$_3$)). Prepared by the general procedure using CuO^{t}Bu (55 mg, 0.40 mmol), dippNacNac^{Me}(H) (167 mg, 0.399 mmol), and PPh$_3$ (47 mg, 0.18 mmol). The mixture was stirred at 60 °C for 48 h. Yield: 47 mg (53%). ^{1}H NMR (400 MHz, C_6D_6): δ (ppm) 7.05–7.15 (m, 6H, Ar*H*), 6.84–6.97 (m, 15H, Ar*H*), 5.13 (s, 1H, N–C(CH$_3$)=C*H*–C(CH$_3$)=N), 3.60 (hept, *J* = 6.9 Hz, 4H, −C*H*(CH$_3$)$_2$), 1.86 (s, 6H, N–C(C*H*$_3$)=CH–C(C*H*$_3$)=N), 1.23 (d, *J* = 6.9 Hz, 12H, −CH(C*H*$_3$)$_2$), 0.82 (d, *J* = 6.8 Hz, 12H, −CH(C*H*$_3$)$_2$). ^{31}P{^{1}H} NMR (162 MHz, C_6D_6): δ (ppm) 3.6 (s).

Cu9 (Cu(dippNacNac^{Me})(PPh$^{OMe}_3$)). Prepared by the general procedure using CuO^{t}Bu (41 mg, 0.30 mmol), dippNacNac(H) (126 mg, 0.301 mmol), and PPh$^{OMe}_3$ (42 mg, 0.12 mmol). The mixture was stirred at room temperature for 48 h. Yield: 52 mg (54%). ^{1}H NMR (400 MHz, C_6D_6): δ (ppm) 7.07–7.14 (m, 6H, Ar*H*), 6.89–6.93 (m, 6H, Ar*H*), 6.57–6.60 (m, 6H, Ar*H*), 5.14 (s, 1H, N–C(CH$_3$)=C*H*–C(CH$_3$)=N), 3.65 (hept, *J* = 6.9 Hz, 1H), −C*H*(CH$_3$)$_2$), 3.26 (s, 9H, OC*H*$_3$), 1.88 (s, 6H, C(C*H*$_3$)=CH–C(C*H*$_3$)=N), 1.26 (d, *J* = 6.8 Hz, 12H, −CH(C*H*$_3$)$_2$), 0.91 (d, *J* = 6.9 Hz, 12H, –CH(C*H*$_3$)$_2$). ^{31}P{^{1}H} NMR (162 MHz, C_6D_6): δ (ppm) −0.28 (s).

Author Contributions

Ashish Kumar: formal analysis, investigation, validation, visualization, writing – original draft, writing – review & editing. Dooyoung Kim: conceptualization, formal analysis, investigation, validation, visualization, writing – review & editing. Giao Nguyen: formal analysis, investigation, validation, visualization, writing – review & editing. Chenggang Jiang: formal analysis, writing – review & editing. Soumi Chakraborty: formal analysis, visualization, writing – review & editing. Thomas S. Teets: conceptualization, formal analysis, funding acquisition, project administration, supervision, visualization, writing – review & editing.

Conflicts of interest

There are no conflicts to declare.

Acknowledgements

This work was supported by the U.S. Department of Energy (DOE), Office of Science, Office of Basic Energy Sciences, CSGB Division under Award # DE-SC0023394. G. N. thanks the University of Houston Energy Scholars Program for a research fellowship.

References

1 L. Wang, *Catalysts*, 2022, **12**, 919.
2 D. Kim, V. Q. Dang and T. S. Teets, *Chem. Sci.*, 2024, **15**, 77–94.
3 T. S. Teets and D. G. Nocera, *Chem. Commun.*, 2011, **47**, 9268–9274.
4 T. R. Cook, D. K. Dogutan, S. Y. Reece, Y. Surendranath, T. S. Teets and D. G. Nocera, *Chem. Rev.*, 2010, **110**, 6474–6502.
5 F. Bella, C. Gerbaldi, C. Barolo and M. Grätzel, *Chem. Soc. Rev.*, 2015, **44**, 3431–3473.
6 B. Pashaei, H. Shahroosvand, M. Graetzel and M. K. Nazeeruddin, *Chem. Rev.*, 2016, **116**, 9485–9564.
7 D. A. Nicewicz and D. W. C. MacMillan, *Science*, 2008, **322**, 77–80.

8 J. M. R. Narayanam, J. W. Tucker and C. R. J. Stephenson, *J. Am. Chem. Soc.*, 2009, **131**, 8756–8757.
9 M. A. Ischay, M. E. Anzovino, J. Du and T. P. Yoon, *J. Am. Chem. Soc.*, 2008, **130**, 12886–12887.
10 S. Cerfontaine, S. A. M. Wehlin, B. Elias and L. Troian-Gautier, *J. Am. Chem. Soc.*, 2020, **142**, 5549–5555.
11 E. D. Nacsa and D. W. C. MacMillan, *J. Am. Chem. Soc.*, 2018, **140**, 3322–3330.
12 C. Kerzig, X. Guo and O. S. Wenger, *J. Am. Chem. Soc.*, 2019, **141**, 2122–2127.
13 J.-H. Shon, D. Kim, M. D. Rathnayake, S. Sittel, J. Weaver and T. S. Teets, *Chem. Sci.*, 2021, **12**, 4069–4078.
14 V. Q. Dang and T. S. Teets, *Chem. Sci.*, 2023, **14**, 9526–9532.
15 C. Fischer, C. Kerzig, B. Zilate, O. S. Wenger and C. Sparr, *ACS Catal.*, 2020, **10**, 210–215.
16 J. Lu, B. Pattengale, Q. Liu, S. Yang, W. Shi, S. Li, J. Huang and J. Zhang, *J. Am. Chem. Soc.*, 2018, **140**, 13719–13725.
17 J. C. Theriot, C.-H. Lim, H. Yang, M. D. Ryan, C. B. Musgrave and G. M. Miyake, *Science*, 2016, **352**, 1082–1086.
18 E. R. Sauvé, D. M. Mayder, S. Kamal, M. S. Oderinde and Z. M. Hudson, *Chem. Sci.*, 2022, **13**, 2296–2302.
19 H. Takeda, Y. Monma and O. Ishitani, *ACS Catal.*, 2021, **11**, 11973–11984.
20 L. A. Büldt and O. S. Wenger, *Angew. Chem. Int. Ed.*, 2017, **56**, 5676–5682.
21 A. Aydogan, R. E. Bangle, A. Cadranel, M. D. Turlington, D. T. Conroy, E. Cauët, M. L. Singleton, G. J. Meyer, R. N. Sampaio, B. Elias and L. Troian-Gautier, *J. Am. Chem. Soc.*, 2021, **143**, 15661–15673.
22 J. A. Kübler, B. Pfund and O. S. Wenger, *JACS Au*, 2022, **2**, 2367–2380.
23 J. K. McCusker, *Science*, 2019, **363**, 484–488.
24 C. Förster and K. Heinze, *Chem. Soc. Rev.*, 2020, **49**, 1057–1070.
25 C. Wegeberg and O. S. Wenger, *JACS Au*, 2021, **1**, 1860–1876.
26 M. T. Miller, P. K. Gantzel and T. B. Karpishin, *Inorg. Chem.*, 1998, **37**, 2285–2290.
27 M. Iwamura, S. Takeuchi and T. Tahara, *J. Am. Chem. Soc.*, 2007, **129**, 5248–5256.
28 M. W. Mara, K. A. Fransted and L. X. Chen, *Coord. Chem. Rev.*, 2015, **282–283**, 2–18.
29 M. Iwamura, S. Takeuchi and T. Tahara, *Acc. Chem. Res.*, 2015, **48**, 782–791.
30 T. Li, J. Schaab, P. I. Djurovich and M. E. Thompson, *J. Mater. Chem. C*, 2022, **10**, 4674–4683.
31 C. N. Muniz, J. Schaab, A. Razgoniaev, P. I. Djurovich and M. E. Thompson, *J. Am. Chem. Soc.*, 2022, **144**, 17916–17928.
32 C. N. Muniz, C. A. Archer, J. S. Applebaum, A. Alagaratnam, J. Schaab, P. I. Djurovich and M. E. Thompson, *J. Am. Chem. Soc.*, 2023, **145**, 13846–13857.
33 Z. Mao, H. Chao, Z. Hui, C. Che, W. Fu, K. Cheung and N. Zhu, *Chem. – Eur. J.*, 2003, **9**, 2885–2894.
34 M. Hashimoto, S. Igawa, M. Yashima, I. Kawata, M. Hoshino and M. Osawa, *J. Am. Chem. Soc.*, 2011, **133**, 10348–10351.
35 K. Lee, P.-N. Lai, R. Parveen, C. M. Donahue, M. M. Wymore, B. A. Massman, B. Vlaisavljevich, T. S. Teets and S. R. Daly, *Chem. Commun.*, 2020, **56**, 9110–9113.
36 D. Kakizoe, M. Nishikawa, Y. Fujii and T. Tsubomura, *Dalton Trans.*, 2017, **46**, 14804–14811.
37 X. Li, J. Ding, W. Jin and Y. Cheng, *Inorganica Chim. Acta*, 2009, **362**, 233–237.
38 J. Nitsch, C. Kleeberg, R. Fröhlich and A. Steffen, *Dalton Trans.*, 2015, **44**, 6944–6960.
39 C.-C. Chou, H.-J. Liu and L. Hung-Chieh Chao, *Chem. Commun.*, 2009, 6382.
40 T. Lu, J.-Y. Wang, L.-X. Shi, Z.-N. Chen, X.-T. Chen and Z.-L. Xue, *Dalton Trans.*, 2018, **47**, 6742–6753.
41 M. Osawa, *Chem. Commun.*, 2014, **50**, 1801.
42 Y.-C. Tsai, *Coord. Chem. Rev.*, 2012, **256**, 722–758.
43 D. Kim, T. G. Gray and T. S. Teets, *Chem. Commun.*, 2022, **58**, 11446–11449.
44 D. Kim and T. S. Teets, *Polyhedron*, 2024, **248**, 116748.
45 D. Kim, M. C. Rosko, V. Q. Dang, F. N. Castellano and T. S. Teets, *Inorg. Chem.*, 2023, **62**, 16759–16769.
46 D. Kim, M. C. Rosko, F. N. Castellano, T. G. Gray and T. S. Teets, *J. Am. Chem. Soc.*, 2024, **146**, 19193–19204.
47 D. Kim and T. S. Teets, *J. Am. Chem. Soc.*, 2024, **146**, 16848–16855.
48 A. G. Orpen and N. G. Connelly, *Organometallics*, 1990, **9**, 1206–1210.
49 A. Vogler and H. Kunkely, *Coord. Chem. Rev.*, 2002, **230**, 243–251.
50 J. T. York, V. G. Young and W. B. Tolman, *Inorg. Chem.*, 2006, **45**, 4191–4198.
51 A. M. Reynolds, E. A. Lewis, N. W. Aboelella and W. B. Tolman, *Chem Commun*, 2005, 2014–2016.
52 R. M. Maya, A. Maity and T. S. Teets, *Organometallics*, 2016, **35**, 2890–2899.
53 M. K. Eggleston, D. R. McMillin, K. S. Koenig and A. J. Pallenberg, *Inorg. Chem.*, 1997, **36**, 172–176.
54 C. E. McCusker and F. N. Castellano, *Inorg. Chem.*, 2013, **52**, 8114–8120.
55 M. C. Rosko, K. A. Wells, C. E. Hauke and F. N. Castellano, *Inorg. Chem.*, 2021, **60**, 8394–8403.
56 A. B. Pangborn, M. A. Giardello, R. H. Grubbs, R. K. Rosen and F. J. Timmers, *Organometallics*, 1996, **15**, 1518–1520.
57 T. Tsuda, T. Hashimoto and T. Saegusa, *J. Am. Chem. Soc.*, 1972, **94**, 658–659.
58 L.-M. Tang, Y.-Q. Duan, X.-F. Li and Y.-S. Li, *J. Organomet. Chem.*, 2006, **691**, 2023–2030.
59 I. El-Zoghbi, S. Latreche and F. Schaper, *Organometallics*, 2010, **29**, 1551–1559.
60 M. Stender, R. J. Wright, B. E. Eichler, J. Prust, M. M. Olmstead, H. W. Roesky and P. P. Power, *J. Chem. Soc. Dalton Trans.*, 2001, 3465–3469.
61 K. Suzuki, A. Kobayashi, S. Kaneko, K. Takehira, T. Yoshihara, H. Ishida, Y. Shiina, S. Oishi and S. Tobita, *Phys. Chem. Chem. Phys.*, 2009, **11**, 9850–9860.
62 G. M. Sheldrick, *Acta Crystallogr. A*, 2008, **64**, 112–122.
63 A. D. Becke, *J. Chem. Phys.*, 1993, **98**, 5648–5652.
64 M. J. Frisch, G. W. Trucks, H. B. Schlegel, G. E. Scuseria, M. A. Robb, J. R. Cheeseman, G. Scalmani, V. Barone, G. A. Petersson, H. Nakatsuji, X. Li, M. Caricato, A. V. Marenich, J. Bloino, B. G. Janesko, R. Gomperts, B. Mennucci, H. P. Hratchian, J. V. Ortiz, A. F. Izmaylov, J. L. Sonnenberg, D. Williams-Young, F. Ding, F. Lipparini, F. Egidi, J. Goings, B. Peng, A. Petrone, T. Henderson, D. Ranasinghe, V. G. Zakrzewski, J. Gao, N. Rega, G. Zheng, W. Liang, M. Hada, M. Ehara, K. Toyota, R. Fukuda, J. Hasegawa, M. Ishida, T. Nakajima, Y. Honda, O. Kitao, H. Nakai, T. Vreven, K. Throssell, J. A. Montgomery Jr., J. E. Peralta, F. Ogliaro, M. J. Bearpark, J. J. Heyd, E. N. Brothers, K. N. Kudin, V. N. Staroverov, T. A. Keith, R. Kobayashi, J. Normand, K. Raghavachari, A. P. Rendell, J. C. Burant, S. S. Iyengar, J. Tomasi, M. Cossi, J. M. Millam, M. Klene, C. Adamo, R. Cammi, J. W. Ochterski, R. L. Martin, K. Morokuma, O. Farkas, J. B. Foresman and D. J. Fox, 2016.
65 Y. Yang, M. N. Weaver and K. M. Merz, *J. Phys. Chem. A*, 2009, **113**, 9843–9851.
66 A. Klamt and G. Schüürmann, *J Chem Soc Perkin Trans 2*, 1993, 799–805.

The data supporting this article have been included as part of the Supplementary Information. Crystallographic data for all complexes have been deposited at the CCDC under 2382410–2382413 and 2382415–2382419 and can be obtained from https://www.ccdc.cam.ac.uk.